Mapping Noncovalent Ligand Binding to Stemloop Domains of the HIV-1 Packaging Signal by Tandem Mass Spectrometry

Kevin B. Turner, Nathan A. Hagan, Andrew S. Kohlway, and Daniele Fabris

Department of Chemistry and Biochemistry, University of Maryland Baltimore County, Baltimore, Maryland, USA

The binding modes and structural determinants of the noncovalent complexes formed by aminoglycoside antibiotics with conserved domains of the HIV-1 packaging signal (Ψ-RNA) were investigated using electrospray ionization (ESI) Fourier transform mass spectrometry (FTMS). The location of the aminoglycoside binding sites on the different stemloop structures was revealed by characteristic coverage gaps in the ion series obtained by sustained off-resonance irradiation collision induced dissociation (SORI-CID) of the antibiotic-RNA assemblies. The site positions were confirmed using mutants that eliminated salient structural features of the Ψ-RNA domains. The effects of the mutations on the binding properties of the different substrates served to validate the position of the aminoglycoside site on the wild-type structures. Additional information was provided by docking experiments performed on the different aminoglycoside-stemloop complexes. The results have shown that, in the absence of features disrupting the regular A-helix of the double-stranded stem, aminoglycosides tend to bind in an area situated between the upper stem and the loop regions, as demonstrated for stemloop SL3. The presence of a tandem wobbles motif in SL4 modifies the regular geometry of the upper stem, which does not affect the general site location, but greatly increases its solution binding affinity compared with SL3. The platform motif in SL2 locates the binding site in the stem midsection and confers upon this stemloop an intermediate affinity toward aminoglycosides. In SL3 and SL4, the extensive overlap of the antibiotic site with the region used to bind the nucleocapsid (NC) protein provides the basis for a competition mechanism that could explain the aminoglycoside inhibition of the NC·SL3 and NC·SL4 assemblies. In contrast, the minimal overlap between the aminoglycoside and the NC sites in SL2 accounts for the absence of inhibition of the NC·SL2 complex. (J Am Soc Mass Spectrom 2006, 17, 1401–1411) © 2006 American Society for Mass Spectrometry

During the replication of human immunodeficiency virus type 1 (HIV-1), specific interactions between the packaging signal (Ψ) [1–3] of viral RNA and the nucleocapsid (NC) [4, 5] domain of the Gag polyprotein mediate the vital functions of genome recognition, dimerization and packaging [6]. The relatively low mutation frequency of this ~120 nt stretch of genomic RNA makes the packaging signal a very promising target for the development of new therapeutic strategies to contend with the rapid emergence of drug resistant strains [7, 8]. For this reason, steps have been made toward the identification of possible inhibitors that may bind specific Ψ-RNA structures and disrupt their normal functions [9–11]. In a systematic investigation of classic nucleic acid ligands, we have recently shown that aminoglycosidic antibiotics are not only capable of binding individual domains of Ψ-RNA, but can also inhibit their interactions with NC in a structure-specific fashion [12]. Initial tests to locate the actual binding sites on the different RNA substrates, which is crucial to explain the mechanism of preferential inhibition, were based on the analysis of mutant-ligand complexes performed by electrospray ionization (ESI) [13, 14] and Fourier transform mass spectrometry (FTMS) [15, 16].

The favorable energetics characteristic of ESI enable the analysis of relatively labile noncovalent complexes by mass spectrometry [17–19] and offer the possibility of obtaining valuable information about specific protein–nucleic acid, nucleic acid–nucleic acid, and small ligand–nucleic acid interactions (reviewed in [20] and [21]). The binding selectivity and the stoichiometry of noncovalent complexes formed by DNA [22–28] and RNA [29–32] substrates with a variety of small organic molecules can be determined unambiguously from di-

Published online July 26, 2006

Address reprint requests to Dr. D. Fabris, Department of Chemistry and Biochemistry, University of Maryland Baltimore County, 100 Hilltop Circle, Baltimore, MD 21228, USA. E-mail: fabris@umbc.edu

1044-0305/06/$32.00
doi:10.1016/j.jasms.2006.06.009

Received April 11, 2006
Revised May 29, 2006
Accepted June 6, 2006

rect mass determinations, rather than from curve fitting of bulk data provided by spectroscopic and calorimetric methods. Relative and absolute binding affinities are readily attainable by strategies that rely on the ability of ESI-MS to resolve complexes with very close physical-chemical characteristics, which are not easily discriminated by other established techniques. Competitive binding experiments have been implemented in which multiple ligands are mixed simultaneously with a target substrate to form a distribution of complexes with abundances reflecting the respective binding affinities [33–37]. Rigorous quantitative determinations of dissociation constants (K_ds) have been obtained from titration experiments in which the abundance of free versus bound species in solution was monitored by ESI-MS after each addition of ligand [12, 38–41].

Tandem mass spectrometry has been extensively used to identify the sequence of oligonucleotide samples [42–46] and characterize their covalent modifications [47–51] based on characteristic ions series produced by fragmentation of the nucleic acid backbone. In contrast, gas-phase activation of small ligand-nucleic acid complexes has been more actively pursued to investigate their stability rather than to map the actual binding sites [52–56]. Characteristic dissociation patterns obtained from these precursor ions have been effectively correlated to the nature and selectivity of the binding interaction. In complexes formed by minor groove binders with duplex DNA oligonucleotides, the direct dissociation of the small molecule was found to be less favorable than the unzipping of the complementary strands [52, 53] and the partial fragmentation of their covalent backbone [54]. In complexes involving DNA quadruplex structures, the contrast between strand disassembly and ligand dissociation served to clearly differentiate the binding modes presented by the groove-binder distamycin and the perylene-diimide analog Tel01 [55].

Targeted fragmentation of the phosphodiester backbone has been previously utilized to screen members of combinatorial libraries for their ability to bind specific targets [38, 57]. Based on the observation that RNA and 2′-O-methyl RNA undergo fragmentation 5 to 10 times less efficiently than DNA [58], a chimeric 2′-O-methyl-ribonucleotide corresponding to the bacterial rRNA A-site was synthesized with deoxyadenine mutations located in selected sequence positions to induce facile gas-phase cleavage. The inhibitory effects exerted by ligand interactions on the dissociation of these key deoxynucleotides were subsequently evaluated to identify the candidates that provided specific binding to the desired site(s) [57].

In this report, we have explored the possibility of employing sustained off-resonance irradiation collision induced dissociation (SORI-CID) [59] to map the actual binding sites of aminoglycosidic antibiotics on individual stemloop domains of Ψ-RNA. The validity of the maps provided by the sequencing experiments was tested using mutant substrates in which the putative sites were modified to reduce or eliminate their ability to bind the ligand, rather than to direct the gas-phase fragmentation processes. Docking experiments were also carried out to test whether the regions mapped by SORI-CID would actually present favorable characteristics to support the ligand interaction. In an effort to explain the selective inhibitory effects induced by aminoglycosides on the different NC-stemloop complexes, the binding determinants and the locations of the ligand sites have been discussed in the context of the unique structural features presented by the target RNA stemloops.

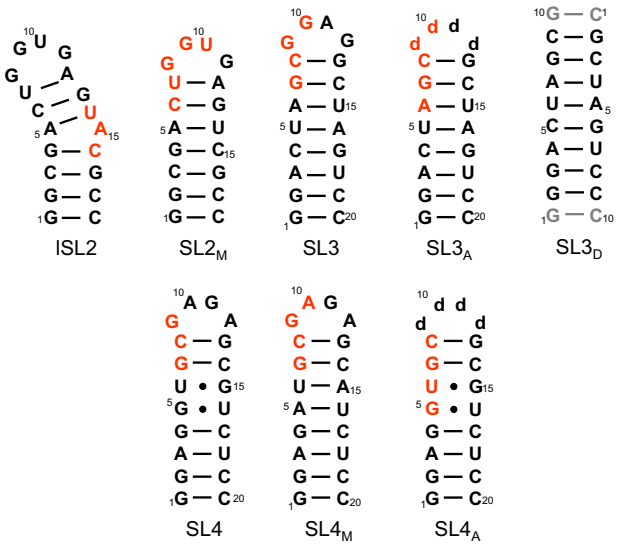

Scheme 1. Sequence and secondary structures of individual stemloops of HIV-1 Ψ-RNA and selected mutants. The letter "d" indicates abasic phosphodeoxyribose spacers. Highlighted in red are the regions identified by tandem mass spectrometry. In gray are the extra GC pairs added to stabilize the $SL3_D$ duplex structure (see the Experimental section).

Experimental

Materials and Methods

Oligo-ribonucleotides matching the sequences of SL2, SL3, and SL4 from the NL4-3 strain of HIV-1 and their respective mutants (Scheme **1**) were purchased from IDT (Coralville, IA). Three additional base pairs were included at the base of the SL4 stem to stabilize its secondary structure. The SL3 duplex ($SL3_D$) was obtained by heat-annealing two individual oligo-ribonucleotides replicating the complementary strands of the SL3 stem. Two GC pairs were added at the ends to increase the stability of the double-stranded structure and match the total number of 20 nucleotides present in the template stemloop construct (Scheme **1**).

Each sample was extensively desalted by ultrafiltration on Centricon YM-3 devices (Millipore, Bedford, MA) using a 100 mM solution of ammonium acetate (pH 7.5). The purity and integrity of each sample were confirmed by ESI-FTMS. The concentration of each stock solution was determined by UV absorbance, using

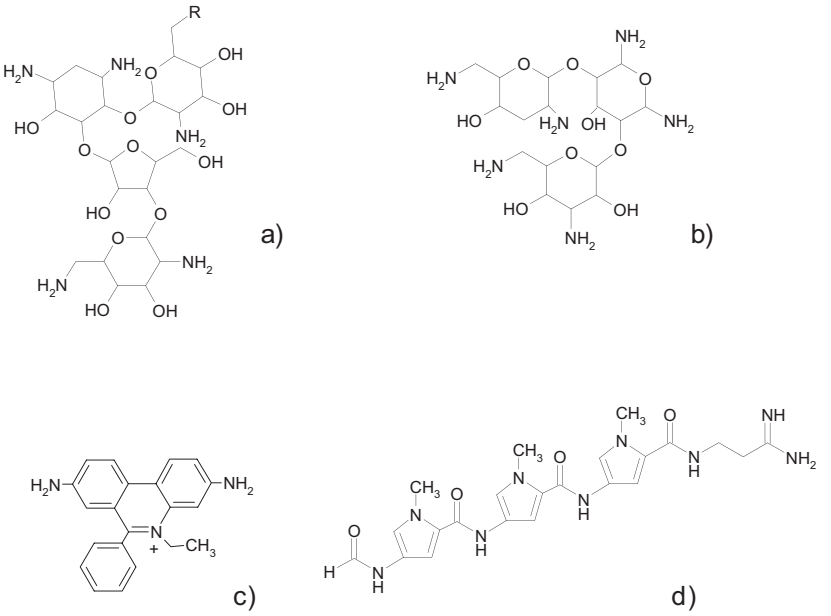

Scheme 2. Structures of nucleic acid ligands employed in the study: (**a**) R = NH_2 neomycin B (NB) and R = OH paromomycin (PR); (**b**) tobramycin (TB); (**c**) ethidium bromide (ET); (**d**) distamycin A (DA).

the following values of molar absorptivity: 190.07 mM^{-1} cm^{-1} for SL2, 201.99 mM^{-1} cm^{-1} for SL3, and 201.99 mM^{-1} cm^{-1} for SL4. Immediately before use, each construct was heated to 95 °C for 3 min and quickly cooled on ice to achieve proper folding of the hairpin structures.

Neomycin B, paromomycin, tobramycin, ethidium bromide, and distamycin A (Scheme **2**) were purchased from Sigma Chemical Co. (St. Louis, MO) and utilized without further purification. Stock solutions were prepared by dissolving weighed amounts of dry material in 100 μL of a 100 mM solution of ammonium acetate (pH 7.5).

The desired ligand-RNA complexes were assembled by mixing appropriate volumes of the respective stock solutions in 100 mM ammonium acetate (pH 7.5), followed by 15 min incubation at room temperature to ensure proper binding. Typical samples consisted of 10 μL solutions containing 3.5 μM RNA. Competitive binding experiments were carried out by mixing equimolar amounts (3.5 μM each) of wild-type and mutant RNA substrates in 100 mM ammonium acetate (pH 7.5). Appropriate volumes of ligand stocks were added to the substrate mixtures to obtain the desired final concentrations, followed by 15 min incubation at room temperature to allow for the multiple binding equilibria to be established. Control experiments performed with longer incubation provided no detectable binding differences.

Mass Spectrometry

Appropriate volumes of isopropanol were added to each sample immediately before analysis to achieve a final 9:1 ratio of aqueous to organic phase. Each nanoelectrospray determination required loading ~ 5 μL analyte solution into an uncoated borosilicate needle with a stainless steel wire inserted from the back end to provide the necessary voltage. All analyses were carried out in negative ion mode on a Bruker Daltonics (Billerica, MA) Apex III 7.0T Fourier transform mass spectrometer equipped with a heated metal desolvation capillary, which was kept at 120 to 150 °C. In tandem experiments, the precursor ion of interest was isolated in the FTMS cell using correlated rf sweeps (CHEF) [60], followed by activation through sustained off-resonance irradiation (SORI) [59]. Frequency offsets below and above the resonant frequency of the precursor ion were sampled to avoid possible "blind spots" in the product spectra [61]. Best results were achieved by using irradiation frequencies that were 600 to 2000 Hz below that of the precursor ion. Off-resonant pulses were typically applied for 250 msec using a 22 to 25 dB attenuation of the maximum power output allowed by the hardware, but lower power experiments were also performed using up to 26 to 31 dB attenuation. Argon was used as the collision gas in pulsed bursts of 100 to 250 ms, which resulted in momentary increases from 1×10^{-11} to 1×10^{-7} mbar of the background pressure measured by the instrument gauge located underneath the ion optics. No attempt was made to determine the actual pressure in the vicinity of the FTMS cell. Twenty-five to fifty scans were typically averaged for each spectrum. All data were acquired in broadband mode and were processed using XMASS 7.0.8 (Bruker). Data reduction and analysis were performed with the aid of MS2Links [51] and the Mongo Oligo Mass Calculator version 2.05 made

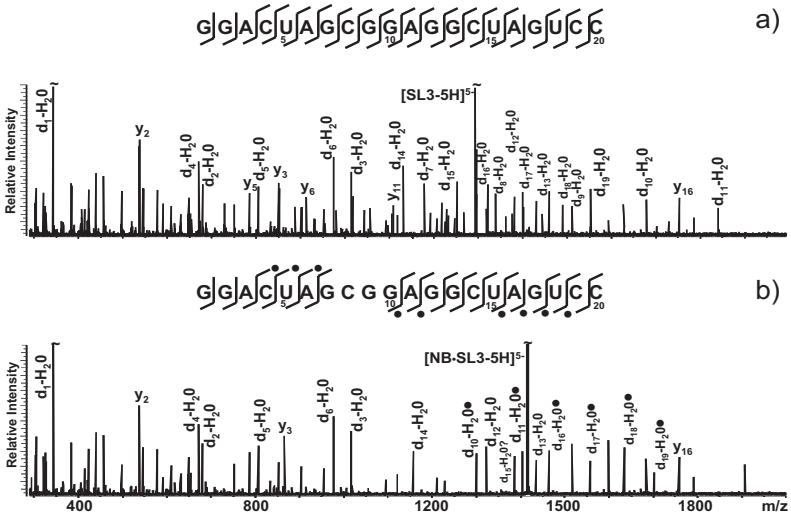

Figure 1. SORI-CID and fragmentation patterns of (**a**) unbound SL3 and (**b**) NB·SL3 assembly. The precursors were quintuply charged anions with *m/z* 1290.59 and 1413.53, respectively. Complete d-H_2O and y-series ions were observed for SL3 (only the more abundant ions were labeled for clarity). Fragment ions containing bound ligand were labeled with a dot. The NB·SL3 fragmentation pattern displayed protection of the G7:G10 sequence, corresponding to the upper stem and loop region of the 5′ side of the secondary structure.

available by Dr. J. McCloskey at http://medlib.med.utah.edu/masspec/.

Docking Calculations

Docking simulations were performed using Autodock 3.0, with additional help from the Autodocktools package [62]. Neomycin B was docked into each stemloop (PDB:1ESY for SL2, PDB:1BN0 for SL3, and PDB:1JTW for SL4) using the Lamarckian genetic algorithm (LGA). A total of 50 docked structures for each stem loop were generated, 10 at a time, using varying grid sizes ranging from 90 × 90 × 90 to 126 × 126 × 126 and a grid spacing of 0.150 to 0.375 Å. Typical settings employed for this procedure include a population size of 150, a maximum number of 250,000 energy evaluations, a maximum number of 27,000 generations, a mutation rate of 0.02, and a crossover rate of 0.8 [62].

Results and Discussion

In recent work, the stoichiometry and binding affinity of NC for hairpin SL2, SL3, and SL4 of HIV-1 Ψ-RNA (Scheme **1**) were determined directly by ESI-FTMS [63]. Using the same approach, aminoglycosidic antibiotics were later found capable of forming stable noncovalent complexes with all three RNA constructs in the absence of NC, but their effects on the corresponding protein-RNA assemblies were shown to be remarkably different [12]. In fact, addition of the aminoglycoside neomycin B (NB, Scheme **2**) to preformed complexes in solution induced the dissociation of NC·SL4 and NC·SL3, while NC·SL2 was not affected under the same experimental conditions. We proposed that aminoglycosides may compete with NC for binding to unique structural features of the different stemloops. The 3D structures of the RNA hairpins [64–66] and the NC complexes with SL2 and SL3 [67, 68] provided helpful indications on the possible sites of such competition. However, in the absence of direct structural information for the aminoglycoside-stemloop complexes, alternative approaches were explored to identify the location of the drug binding sites on the different RNA constructs.

Tandem Mass Spectrometry of Aminoglycoside-Stemloop Complexes

The effects of aminoglycoside complexation on the gas-phase fragmentation of the stemloop structures were investigated by comparing the results provided by SORI-CID of free and bound RNA samples. The initial substrates produced typical d-H_2O (also described as c) and y series expected from this type of nucleic acid [42, 51, 69, 70], as shown, for example, by the SL3 construct in Figure 1a. No loss of nucleobases was observed, consistent with the fact that cleavage of the N-glycosidic bond in RNA is not associated with fragmentation of the phosphodiester backbone. Additionally, the nearly complete sequence coverage obtained under the selected experimental conditions offered no evidence of possible fragmentation inhibition that could be ascribed to base-pairing between the stem complementary strands.

Activation of the 1:1 complex of neomycin B with SL3 (NB·SL3) induced no direct ligand dissociation under the same conditions, while fragmentation of the oligonucleotide backbone was readily detected (Figure 1b). Characteristic d-H_2O and y products were observed with no base losses, but a distinctive gap in the

sequence coverage was evident between G7 and G10 (G7:G10). The fact that this region is very well represented in the spectrum of free SL3 (see ions d_7-H_2O through d_9-H_2O and y_{11} through y_{14} in Figure 1a) suggests that the observed inhibition of phosphodiester cleavage can be safely ascribed to the presence of ligand. Furthermore, the observation that the majority of the d-H_2O and y ions from the region located 3′ of the protected stretch retained the drug, while none of those from the 5′ side did, provides strong indications that the protection effects can be directly correlated to ligand binding.

In analogous fashion, tandem mass spectrometry was employed to investigate the binding of other aminoglycosides, such as tobramycin (TB) and paromomycin (PR) (Scheme **2**), which shared NB's ability to disrupt the NC·SL3 complex in solution. The binding mode of this class of antibiotics relies on multiple hydrogen bonds and electrostatic interactions, which require the participation of basic functional groups distributed on the flexible 2-deoxystreptamine scaffold [10, 71, 72]. The presence of six amino groups in NB versus only five in TB and PR (Scheme **2**) was considered responsible for the lower dissociation constant determined in solution for NB·SL3 (i.e., 4.2 ± 0.3 μM) than for the other two complexes (i.e., 38.7 ± 3.7 μM and 37.7 ± 1.3 μM, respectively) [12]. However, no significant differences could be noted among the fragmentation patterns produced by the aminoglycoside complexes under similar SORI-CID conditions (not shown). In fact, the ion series obtained from TB·SL3 and PR·SL3 presented the same coverage gap observed for NB·SL3, while only small and inconclusive variations of ligand retention were exhibited by the fragment ions. These results are consistent with the rather diffuse nature of the aminoglycosides binding mode that utilizes several points of contact with the substrate to achieve effective binding. Therefore, tandem experiments are expected to highlight a series of nucleotides in the construct sequence, which are part of a wider surface involved in ligand binding. The fact that all three aminoglycosides in the study appeared to protect the same G7:G10 region confirms the presence of a unique high-affinity site on this stemloop, the boundaries of which may be delimited by these and spatially contiguous bases in the construct secondary structure.

Effects of Binding Mode on Gas-Phase Dissociation

The correlation between binding mode and gas-phase behavior was further investigated using alternative ligand-stemloop assemblies that did not involve significant electrostatic interactions. The intercalator ethidium bromide (ET) was selected for its ability to insert between GC base pairs and induce effective stacking of the planar aromatic systems [73, 74]. The groove-binder distamycin A (DA) was chosen for its reliance on specific H-bonding interactions that are sensitive to perturbations of the minor groove size and geometry [75]. Following SORI-CID, the 1:1 complexes of SL3 with ET and DA provided backbone fragmentation in addition to prominent ligand dissociation (not shown). No gaps in the respective ion series or drug-retaining products were noted, which would have revealed the position of the binding sites. In subsequent experiments, the power of the off-resonant pulse was progressively reduced in an attempt to limit ligand dissociation and highlight its protection effects (see the Experimental section). Even upon significant reduction of the applied power, ET·SL3 and DA·SL3 still dissociated to generate free SL3, while NB·SL3 remained nearly completely intact (Figure 2), thus suggesting a NB·SL3 $\gg$ ET·SL3 $\approx$ DA·SL3 gas-phase stability scale under the selected activation conditions. These results are in striking contrast with the solution dissociation constants determined by titration experiments, corresponding to 1.9 ± 0.2 μM for ET·SL3, 4.2 ± 0.3 μM for NB·SL3, and 28.5 ± 4.7 μM for DA·SL3 [12]. The drastic drop of ET·SL3 in the stability scale could be explained by the entropic penalty associated with desolvation, which is expected to be sizeable for intercalating interactions. More significantly, the SORI-CID process itself could be affecting the structural features of the RNA substrate, which sustain the actual intercalation and groove binding. This explanation would involve the dissociation of the base pairs in the hairpin double-stranded stem, in analogy with the melting of duplex oligonucleotides observed under different collisional activation [76, 77].

A duplex RNA mimicking the double-stranded stem of SL3 ($SL3_D$, Scheme **1**) was synthesized to overcome the fact that denaturation of a hairpin secondary structure is a mass silent process. The stable noncovalent complexes obtained by mixing $SL3_D$ with the different ligands were subjected to SORI-CID at the lower power described above. Unlike equivalent complexes of the stemloop construct, ET·$SL3_D$ and DA·$SL3_D$ did not show direct ligand dissociation to regenerate intact $SL3_D$, but instead produced ions corresponding to the individual strands with no retention of ligand (Figure 3a and b). The NB·$SL3_D$ complex did not show direct ligand release either, but NB was found to remain associated to the melted strands with a preference for the 5′-oligonucleotide (Figure 3c). The absence of unbound intact $SL3_D$ in any of these spectra provides strong support to the suggested connection between strand melting and ligand dissociation. In fact, denaturation is a very effective way to eliminate the base-pairing and helical structure necessary for intercalation and minor groove binding. In the case of aminoglycosides, the strong electrostatic component of their binding mode can overcome the loss of structural context and preserve their association with the single-stranded products.

Applied to the stemloop assemblies, this mechanism would involve dissociation of base pairs and defolding of the RNA secondary structure, which would alternatively result in the release of intercalators and groove

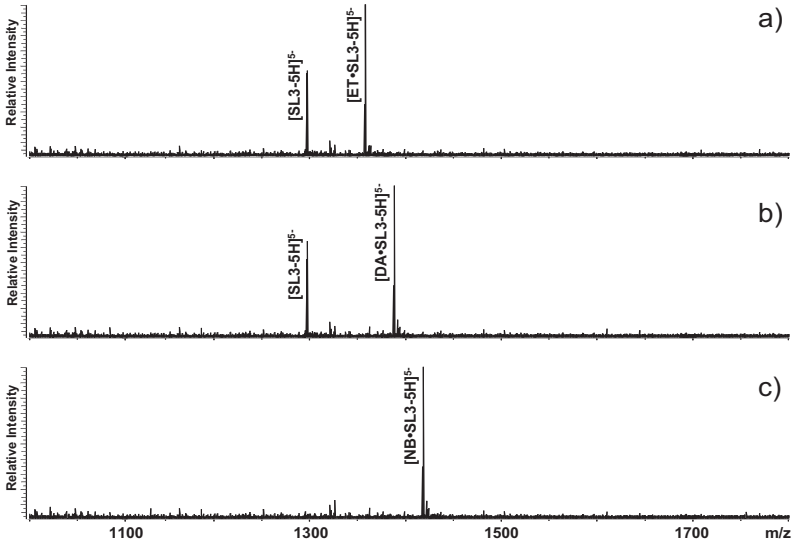

Figure 2. Lower power SORI-CID of (**a**) ET·SL3, (**b**) DA·SL3, and (**c**) NB·SL3 assembly (see the Experimental section). All precursors were quintuply charged anions with *m/z* 1353.62, 1386.81, and 1413.53, respectively. While ET·SL3 and DA·SL3 displayed direct dissociation of ligand and minimal fragmentation, NB·SL3 showed no ligand dissociation and minimal fragmentation under the same experimental conditions.

binders, or retention of aminoglycosides by the single-stranded sequences that were originally part of the stem. In support of this explanation, the preferential association of NB with the 5′ moiety of the linearized hairpin sequence (Figure 1b) was in excellent agreement with the asymmetric results provided by the melting of the NB·SL3$_D$ assembly, in which NB was found to remain preferentially bound to the 5′ strand (Figure 3c). The greater number of Gs in this region is likely to be the cause for the asymmetric dissociation based on the high gas-phase basicity characteristic of this nucleobase [78]. These observations constitute further evidence of the electrostatic character of aminoglycoside binding. It is probably due to the stability of such interactions, which preserved "memory" of the initial structural context, that information provided by backbone fragmentation could be effectively used to map the position of the aminoglycoside sites. Further investigations will be necessary to elucidate the complex interplay between stemloop melting, ligand binding, and backbone

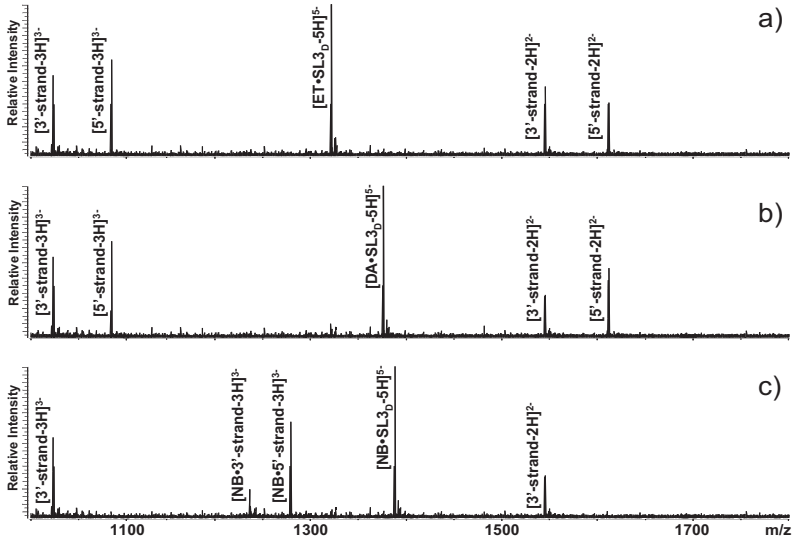

Figure 3. Lower power SORI-CID of (**a**) ET·SL3$_D$, (**b**) DA·SL3$_D$, and (**c**) NB·SL3$_D$ assembly (see the Experimental section). All precursors were quintuply charged anions with *m/z* 1328.42, 1361.63, and 1388.26, respectively. The ET·SL3$_D$ and DA·SL3$_D$ assemblies displayed duplex melting, no direct ligand dissociation, and no residual association of ligand to the melted strands. In contrast, NB·SL3$_D$ showed duplex melting and no direct ligand dissociation, but the ligand remained associated to the melted strands.

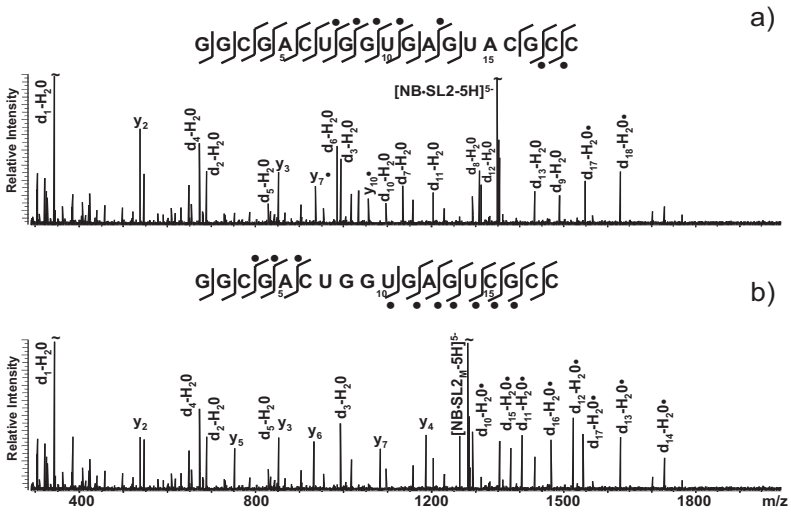

Figure 4. SORI-CID and fragmentation patterns of (**a**) NB·SL2 and (**b**) NB·$SL2_M$ assembly. Both precursors were quintuply charged anions with *m/z* 1293.64 and 1281.83, respectively. Fragment ions containing bound ligand were labeled with a dot. The former displayed protection of U14:C16, located below the base-triple platform on the 3′ stem. The latter showed protection of C6:U10, in the upper stem and loop region on the 5′ side of the secondary structure.

fragmentation, which determine the observed protection effects.

Structural Determinants of Aminoglycoside Binding

Tandem mass spectrometry was employed to investigate the binding of aminoglycosides with the other Ψ-RNA stemloops, SL2, and SL4. Coverage gaps in the fragment ion series produced by these complexes, which were not observed in the spectra of their respective unbound substrates, were used to identify the regions of ligand interaction as described above. The locations inferred from SORI-CID experiments were compared with those obtained from simulations in which NB was docked in different positions of the stemloop structures and the stability of the resulting complexes was scored according to estimations of binding free-energy provided by different algorithms included in Autodock 3.0 [62].

In the case of NB·SL2 (Figure 4a), the protected U14:C16 sequence included two nucleotides that were part of a base-triple platform located in the middle of the double-stranded stem [64]. Base mismatches in the stemloop helical region introduce a kink that situates the nucleobase of U14 on the same plane with those of A5 and A15 to complete the platform structure. In addition, this arrangement creates a highly negative area on the major groove surface below the platform, which could establish strong interactions with the basic aminoglycosides (Figure 5a). This hypothesis was tested using an RNA mutant in which the platform motif was eliminated by A15 deletion ($SL2_M$, Scheme **1**). SORI-CID of the NB·$SL2_M$ complex showed a dramatic shift in the protection profile, which pointed toward the C6:U10 region as the new putative site (Figure 4b). Considering that this mutant presented an approximate 50% decrease of the solution-phase affinity for NB, as shown by previous competitive binding experiments [12], these results strongly support the platform motif as the location of the high-affinity site on the wild-type SL2 structure (Figure 5a). Further support was provided by the fact that the complex with NB bound below the platform consistently provided the lowest estimates of binding free-energy among the different structures obtained by the docking simulations (Figure 5a).

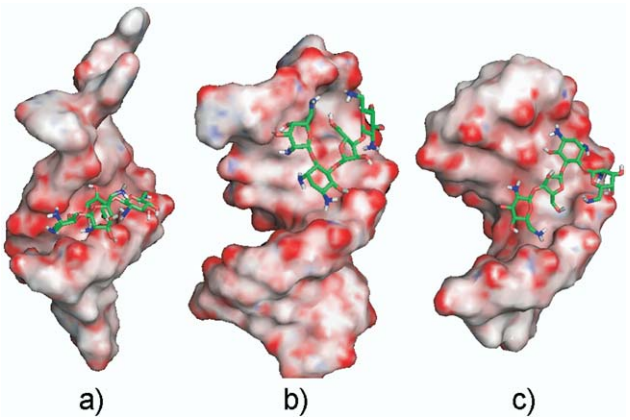

Figure 5. Electrostatic surface of (**a**) SL2 (PDB:1ESY), (**b**) SL3 (PDB:1BN0), and (**c**) SL4 (PDB:1JTW) with docked NB antibiotic. The surfaces were calculated in a 100 mM salt environment utilizing Delphi [81] and visualized in Pymol [82]. The red coloring marks highly electronegative regions. The positions occupied by NB were obtained by Autodock 3.0 [62] (see the Experimental section) and correspond to the assemblies that provided the lowest estimates of free binding energy.

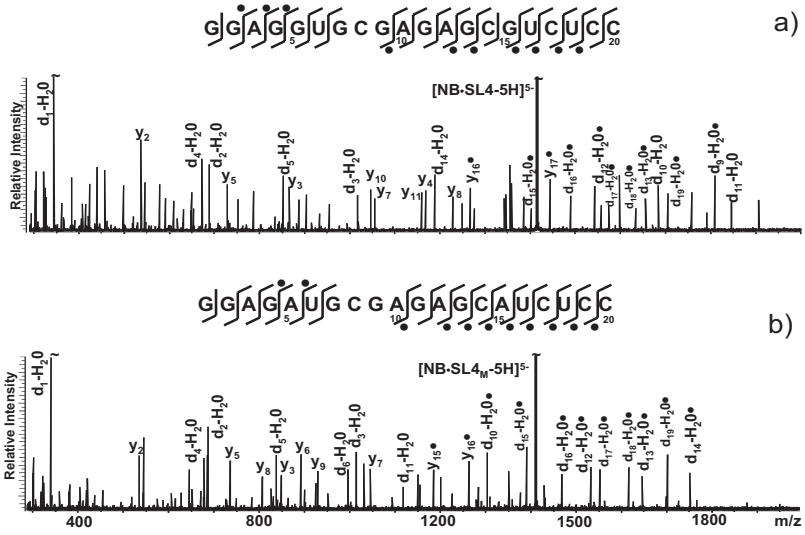

Figure 6. SORI-CID and fragmentation patterns of (**a**) NB·SL4 and (**b**) NB·$SL4_M$ assembly. Both precursors were quintuply charged anions with *m/z* 1416.64 and 1404.29, respectively. Fragment ions containing bound ligand were labeled with a dot. The former displayed protection of G7:G9, located in the upper stem and loop region of the 5′ side of the secondary structure. The latter showed protection G7:A10, corresponding to the upper stem and loop region of the 5′ side.

In the case of NB·SL4 (Figure 6a), the G7:G9 sequence protected from fragmentation is situated between two structurally significant motifs [66]. The first is the GAGA tetraloop that adopts the classic GNRA-type fold (R = purine, *N* = G, C, A, or U) [79]. This structure is characterized by extensive base stacking, which reduces the flexibility of the unpaired bases and adds stability to the hairpin fold. The second motif corresponds to the tandem GU wobbles found in the stem, which involve noncanonical base-pairing interactions that force the double-stranded stem to assume a wider and less compact conformation [80]. This combination creates a wider and more negative major groove, which was clearly identified as the most ideal region for aminoglycoside binding by the docking simulations (Figure 5c).

Following the strategy described above, sequence mutations were employed to systematically modify the distinctive features of this stemloop. Construct $SL4_M$ was prepared by replacing G5 and G15 with A, thus eliminating the tandem wobbles and restoring a regular A-type helix (Scheme **1**). Mutant $SL4_A$ replaced all four loop nucleotides with abasic phosphodeoxyribose spacers (d), thus erasing the possibility of interactions with nucleobases of the GNRA motif. Analyzed by SORI-CID, the NB·$SL4_M$ assembly showed fragmentation inhibition in the G7:A10 region (Figure 6b), which represents a moderate extension of the putative binding site toward the loop structure as compared to wild-type SL4. In contrast, the NB·$SL4_A$ complex displayed protection of the G5:d9 sequence (not shown), which corresponds to a more pronounced extension of the site toward the tandem wobbles motif. Competitive binding experiments in solution provided a relative affinity scale of SL4 > $SL4_A$ ≫ $SL4_M$, which clearly indicates that the wobbles mutations has the most significant impact on the solution stability of NB binding. Correlating the site maps with the respective affinities in solution clearly identifies the high-affinity site with the upper stem region of wild-type SL4, where effective ligand interactions can be established with the wobbles functional groups and additional stabilization can be offered by the loop bases, as indicated also by the docking results (Figure 5c).

The results obtained from mutant stemloops provided important information regarding the structural determinants of aminoglycoside binding. A consequence of removing the platform and wobble motifs was the creation of hairpin structures that included regular A-helical stems analogous to that of SL3 [65]. The fact that the putative sites on $SL2_M$, $SL4_M$, and SL3 were all localized at the boundary between upper stem and loop is not coincidental, and should be ascribed to the high structural homology presented by these constructs. Not surprisingly, these samples provided very similar affinities toward NB in competitive binding experiments in solution [12]. As shown by the electrostatic surface of SL3 (Figure 5b), this region presents many opportunities for interactions with positively charged aminoglycosides. In addition, the flexibility of the loop and aminoglycoside backbones is expected to facilitate the positioning of the respective functional groups to maximize the binding interactions. Consistent with these observations, the docking experiments provided several alternative structures within a relatively narrow range of estimated binding energies. In SL4, the position of the GU wobbles has minimal effects on the actual site location, which remains situated at the upper stem-loop boundary. However, this motif in-

troduces a broader negative surface that is very favorable to aminoglycoside binding (Figure 5c). The vicinity of the loop structures enables further stabilization, which contributes to the highest solution affinity among the wild-type stemloops. In SL2, the base-triple platform motif offers an excellent negative surface for aminoglycoside binding (Figure 5a). However, its location in the stem midsection precludes any additional stabilization from loop interactions, which results in an intermediate binding affinity among the stemloops [12].

Conclusions

The noncovalent binding of aminoglycosides with stemloop substrates produces localized inhibitory effects on the normal backbone fragmentation of the RNA strand by SORI-CID. The gap in sequence coverage provided by the characteristic ion series identifies stretches of nucleotides that are part of the aminoglycoside binding site. In covalent adducts, the contacts between substrates and modifiers are clearly defined by permanent covalent bonds. Therefore, the position of modified bases can be unambiguously revealed by tandem mass spectrometry. In contrast, noncovalent adducts involve interactions that may not be as narrowly localized, but may be rather diffuse in nature. Therefore, tandem mass spectrometry is expected to point toward a range of nucleotides within the substrate sequence and some knowledge of the substrate secondary structure may still be necessary to complete the picture. Aminoglycoside binding relies on multiple noncovalent contacts with different functional groups on the RNA surface. The broad area corresponding to the possible interface and the relative flexibility of the RNA and ligand structures virtually ensure that different populations coexist for each assembly, which present alternative combinations of contacts within the specific site. The ability to obtain this type of information is highly dependent on the binding mode of the ligand under investigation, which has to withstand at least in part to the denaturing effects of collisional activation on the ligand-substrate assembly. The mechanism by which the binding interactions translate into fragmentation protection will be the object of future study.

The maps obtained for the different stemloops are consistent with the results of docking simulations and with the binding properties revealed by prior investigations. The high-affinity site of SL3 has been shown to span the boundary between the double-stranded stem and the single-stranded loop, in a location shared by mutant stemloops that lack of structural features disrupting their A-helical stems. The regular geometry of the upper stem is affected by the presence of the tandem wobbles in SL4. Rather than displacing the site away from the loop, this motif provides an excellent surface for aminoglycoside binding, which is still within reach of the loop structures. The combined effects result in a dramatic increase of the stemloop affinity toward aminoglycosides. More significantly, it is important to note that the site position in SL3 and SL4 falls within the larger region occupied by the NC protein in the NC·SL3 [68] and possibly NC·SL4 complex, for which there is no high-resolution structure. The extensive overlap between the antibiotic site and the protein footprint on these RNA domains provides the basis for a competition mechanism that could explain the aminoglycoside inhibition of these NC-stemloop assemblies. In contrast, the location of the aminoglycoside site beneath the platform motif in SL2 enables only a marginal overlap with the protein position in NC·SL2 [67] and is consistent with the inability of the antibiotics to disrupt this assembly. Future work will focus on studying the effects of aminoglycoside antibiotics and other small molecule ligands on the interactions between NC and the full length Ψ-RNA to support the development of new antiviral strategies. This investigation will also offer the opportunity to test the applicability of the method to larger RNA structures that may include multiple sites and in which divalent metals (i.e., Mg^{2+}) may contribute directly or indirectly to shape the binding sites.

Acknowledgments

This research was funded by the National Institutes of Health (R01-GM643208) and the National Science Foundation (CHE-0439067). NAH was also supported by an NIH Chemistry Biology Interface Training Fellowship (T32-GM066706).

References

1. Lever, A. M.; Göttlinger, H. T.; Haseltine, W. A.; Sodroski, J. G. Identification of a sequence required for efficient packaging of human immunodeficiency virus type 1 RNA into virions. *J. Virol.* **1987,** *63,* 4085–4087.
2. Linial, M. L.; Miller, A. D.; Retroviral, R. N. A. packaging: Sequence requirements and implications. *Curr. Top. Microbiol. Immunol.* **1990,** *157,* 25–52.
3. Darlix, J. L.; Gabus, C.; Nugeyre, M. T.; Clavel, F.; Barre-Sinussi, F. Cis elements and trans-acting factors involved in the RNA dimerization of the human immunodeficiency virus HIV-1. *J. Mol. Biol.* **1990,** *216,* 689–699.
4. Dickson, C.; Eisenman, R.; Fan, H.; Hunter, E.; Reich, N. 1985; Protein biosynthesis and assembly. Weiss, R.; Ed.; In RNA Tumor Viruses; pp 513–648.Cold Spring Harbor Laboratory Press: Plainview, NY,
5. Darlix, J. L.; Lapadat-Tapolsky, M.; de Roquigny, H.; Roques, B. P. First glimpse at structure–function relationships of the nucleocapsid protein of retroviruses. *J. Mol. Biol.* **1995,** *254,* 523–537.
6. Coffin, J. M.; Hughes, S. H.; Varmus, H. In *Retroviruses*; Cold Spring Harbor Laboratory Press: Plainview, NY, 1997.
7. Johnson, V. A.; Brun-Vezinet, F.; Clotet, B.; Conway, B.; Kuritzkes, D. R.; Pillay, D.; Shapiro, J. M.; Telenti, A.; Richman, D. D. Update of the drug resistance mutations in HIV-1: 2005. *Top. HIV Med.* **2005,** *13,* 51–57.
8. Yusa, K.; Kavlick, M. F.; Kosalaraksa, P.; Mitsuya, H. HIV-1 acquires resistance to two classes of antiviral drugs through homologous recombination. *Antivirus Res.* **1997,** *36,* 179–189.
9. McPike, M. P.; Sullivan, J. M.; Goodisman, J.; Dabrowiak, J. C. Footprinting, circular dichroism, and UV melting studies on neomycin B binding to the packaging region of human immunodeficiency virus type-1 RNA. *Nucleic Acids Res.* **2002,** *30,* 2825–2831.
10. Ennifar, E.; Paillart, J. C.; Marquet, R.; Ehresmann, B.; Ehresmann, C.; Dumas, P.; Walter, P. HIV-1 RNA dimerization initiation site is structurally similar to the ribosomal A site and binds aminoglycoside antibiotics. *J. Biol. Chem.* **2003,** *278,* 2723–2730.
11. McPike, M. P.; Goodisman, J.; Dabrowiak, J. C. Footprinting and circular dichroism studies on paromomycin binding to the packaging region of human immunodeficiency virus type-1. *Bioorg. Med. Chem.* **2002,** *10,* 3663–3672.

12. Turner, K. B.; Hagan, N. A.; Fabris, D. Inhibitory effects of archetypical nucleic acid ligands on the interactions of HIV-1 nucleocapsid protein with elements of Ψ-RNA. *Nucleic Acids Res.* **2006,** *34,* 1305–1316.
13. Yamashita, M.; Fenn, J. B. Electrospray ion source. Another variation on the free-jet theme. *J. Phys. Chem.* **1984,** *88,* 4671–4675.
14. Aleksandrov, M. L.; Gall, L. N.; Krasnov, V. N.; Nikolaev, V. I.; Pavlenko, V. A.; Shkurov, V. A.Extraction of ions from solutions under atmospheric pressure: A method of mass spectrometric analysis of bioorganic compounds.Doklady Akademii Nauk.2773791984383
15. Comisarow, M. B.; Marshall, A. G. Fourier transform ion cyclotron resonance. *Chem. Phys. Lett.* **1974,** *25,* 282–283.
16. Marshall, A. G.; Hendrickson, C. L.; Jackson, G. S. Fourier transform ion cyclotron resonance mass spectrometry: A primer. *Mass Spectrom. Rev.* **1998,** *17,* 1–35.
17. Ganem, B.; Li, Y. T.; Henion, J. D. Detection of noncovalent receptor-ligand complexes by mass spectrometry. *J. Am. Chem. Soc.* **1991,** *113,* 6294–6296.
18. Ganguly, A. K.; Pramanik, B. N.; Tsarbopoulos, A.; Covey, T. R.; Huang, E.; Fuhrman, S. A. Mass spectrometric detection of the noncovalent GDP-bound conformational state of the human H-*ras* protein. *J. Am. Chem. Soc.* **1992,** *114,* 6559–6560.
19. Loo, J. A. Studying noncovalent protein complexes by electrospray ionization mass spectrometry. *Mass Spectrom. Rev.* **1997,** *16,* 1–23.
20. Beck, J. L.; Colgrave, M. L.; Ralph, S. F.; Sheil, M. M. Electrospray ionization mass spectrometry of oligonucleotide complexes with drugs, metals, and proteins. *Mass Spectrom. Rev.* **2001,** *20,* 61–87.
21. Hofstadler, S. A.; Griffey, R. H. Analysis of noncovalent complexes of DNA and RNA by mass spectrometry. *Chem. Rev.* **2001,** *101,* 377–390.
22. Hsieh, Y. L.; Li, Y. T.; Henion, J. D.; Ganem, B. Studies of noncovalent interactions of actinomycin D with single-stranded oligodeoxynucleotides by ion spray mass spectrometry and tandem mass spectrometry. *Biol. Mass Spectrom.* **1994,** *23,* 272–276.
23. Gale, D. C.; Goodlett, D. R.; Light-Wahl, K. J.; Smith, R. D. Observation of duplex DNA-drug noncovalent complexes by electrospray mass spectrometry. *J. Am. Chem. Soc.* **1994,** *116,* 6027–6028.
24. Triolo, A.; Arcamone, F. M.; Raffaelli, A.; Salvadori, P. Noncovalent complexes between DNA-binding drugs and double-stranded deoxynucleotides: A study by ionspray mass spectrometry. *J. Mass Spectrom.* **1997,** *32,* 1186–1194.
25. Gupta, R.; Kapur, A.; Beck, J. L.; Sheil, M. M. Positive ion electrospray ionization mass spectrometry of double-stranded DNA/drug complexes. *Rapid Commun. Mass Spectrom.* **2001,** *15,* 2472–2480.
26. Carrasco, C.; Rosu, F.; Gabelica, V.; Houssier, C.; De Pauw, E.; Garbay-Jaureguiberry, C.; Roques, B.; Wilson, W. D.; Chaires, J. B.; Waring, M. J.; Bailly, C. Tight binding of the antitumor drug ditercalinium to quadruplex DNA. *Chem. Biochem.* **2002,** *3,* 1235–1241.
27. Rosu, F.; Gabelica, V.; Shin-ya, K.; De Pauw, E. Telomestatin-induced stabilization of the human telomeric DNA quadruplex monitored by electrospray mass spectrometry. *Chem. Commun. (Camb.)* **2003,** *21,* 2702–2703.
28. Rosu, F.; De Pauw, E.; Guittat, L.; Alberti, P.; Lacroix, L.; Mailliet, P.; Riou, J. F.; Mergny, J. L. Selective interaction of ethidium derivatives with quadruplexes: An equilibrium dialysis and electrospray ionization mass spectrometry analysis. *Biochemistry* **2003,** *42,* 10361–10371.
29. Mei, H. Y.; Mack, D.; Galan, A. A.; Halim, N. S.; Heldsinger, A.; Loo, J. A.; Moreland, D. W.; Sannes-Lowery, K. A.; Sharmeen, L.; Truong, H. N.; Czarnik, A. W. Discovery of selective, small-molecule inhibitors of RNA complexes-I. The Tat protein/TAR RNA complexes required for HIV-1 transcription. *Bioorg. Med. Chem.* **1997,** *5,* 1173–1184.
30. Mei, H. Y.; Cui, M.; Heldsinger, A.; Lemrow, S. M.; Loo, J. A.; Sannes-Lowery, K. A.; Sharmeen, L.; Czarnik, A. W. Inhibitors of protein-RNA complexation that target the RNA: Specific recognition of human immunodeficiency virus type 1 TAR RNA by small organic molecules. *Biochemistry* **1998,** *37,* 14204–14212.
31. Griffey, R. H.; Sannes-Lowery, K. A.; Drader, J. J.; Mohan, V.; Swayze, E. E.; Hofstadler, S. A. Characterization of Low-Affinity Complexes between RNA and Small Molecules Using Electrospray Ionization Mass Spectrometry. *J. Am. Chem. Soc.* **2000,** *122,* 9933–9938.
32. Maddaford, S. P.; Motamed, M.; Turner, K. B.; Choi, M. S. K.; Ramnauth, J.; Rakhit, S.; Hudgins, R. R.; Fabris, D.; Johnson, P. E. Identification of a novel noncarbohydrate molecule that binds to the ribosomal A-site RNA. *Bioorg. Med. Chem. Lett.* **2004,** *14,* 5987–5990.
33. Kapur, A.; Beck, J. L.; Sheil, M. M. Observation of daunomycin and nogalamycin complexes with duplex DNA using electrospray ionization mass spectrometry. *Rapid Commun. Mass Spectrom.* **1999,** *13,* 2489–2497.
34. Gabelica, V.; De Pauw, E.; Rosu, F. Interaction between antitumor drugs and a double-stranded oligonucleotide studied by electrospray ionization mass spectrometry. *J. Mass Spectrom.* **1999,** *34,* 1328–1337.
35. Sannes-Lowery, K. A.; Mei, H.-Y.; Loo, J. A. Studying aminoglycoside antibiotic binding to HIV-1 TAR RNA by electrospray ionization mass spectrometry. *Int. J. Mass Spectrom. Ion Processes* **1999,** *193,* 115–122.
36. Hofstadler, S. A.; Sannes-Lowery, K. A.; Crooke, S. T.; Ecker, D. J.; Sasmor, H.; Manalili, S.; Griffey, R. H. Multiplexed screening of neutral mass-tagged RNA targets against ligand libraries with electrospray ionization FTICR MS: A paradigm for high-throughput affinity screening. *Anal. Chem.* **1999,** *71,* 3436–3440.
37. Wan, K. X.; Shibue, T.; Gross, M. L. Noncovalent Complexes between DNA-Binding Drugs and Double-Stranded Oligodeoxynucleotides: A Study by ESI Ion-Trap Mass Spectrometry. *J. Am. Chem. Soc.* **2000,** *122,* 300–307.
38. Griffey, R. H.; Hofstadler, S. A.; Sannes-Lowery, K. A.; Ecker, D. J.; Crooke, S. T. Determinants of aminoglycoside-binding specificity for rRNA by using mass spectrometry. *Proc. Nat. Acad. Sci. U.S.A.* **1999,** *96,* 10129–10133.
39. Sannes-Lowery, K. A.; Griffey, R. H.; Hofstadler, S. A. Measuring dissociation constants of RNA and aminoglycoside antibiotics by electrospray ionization mass spectrometry. *Anal. Biochem.* **2000,** *280,* 264–271.
40. Rosu, F.; Gabelica, V.; Houssier, C.; De Pauw, E., Determination of affinity, stoichiometry, and sequence selectivity of minor groove binder complexes with double-stranded oligodeoxynucleotides by electrospray ionization mass spectrometry. *Nucleic Acids Res,* **2002,***30,*e82.
41. Gooding, K. B.; Higgs, R.; Hodge, B.; Stauffer, E.; Heinz, B.; McKnight, K.; Phipps, K.; Shapiro, M.; Winkler, M.; Ng, W. L.; Julian, R. K. High throughput screening of library compounds against an oligonucleotide substructure of an RNA target. *J. Am. Soc. Mass Spectrom.* **2004,** *15,* 884–892.
42. Cerny, R. L.; Tomer, K. B.; Gross, M. L.; Grotjahn, L. Fast atom bombardment combined with tandem mass spectrometry for determining structures of small oligonucleotides. *Anal. Biochem.* **1987,** *165,* 175–182.
43. McLuckey, S.A.; Habibi-Goudarzi, S. Decompositions of multiply charged oligonucleotide anions. *J. Am. Chem. Soc.* **1993,** *115,* 12085–12095.
44. Little, D. P.; Chorush, R. A.; Spier, J. P.; Senko, M. W.; Kelleher, N. L.; McLafferty, F. W. Rapid sequencing of oligonucleotides by high-resolution mass spectrometry. *J. Am. Chem. Soc.* **1994,** *116,* 4893–4897.
45. Ni, J.; Pomerantz, C.; Rozenski, J.; Zhang, Y.; McCloskey, J. A. Interpretation of oligonucleotide mass spectra for determination of sequence using electrospray ionization and tandem mass spectrometry. *Anal. Chem.* **1996,** *68,* 1989–1999.
46. Limbach, P. A.; Crain, P. F.; McCloskey, J. A. Characterization of oligonucleotides and nucleic acids by mass spectrometry. *Curr. Opin. Biotechnol.* **1995,** *6,* 96–102.
47. Kowalak, J. A.; Pomerantz, S. C.; Crain, P. F.; McCloskey, J. A. A novel method for the determination of post-transcriptional modification in RNA by mass spectrometry. *Nucleic Acids Res.* **1993,** *21,* 4577–4585.
48. Barry, J. P.; Vouros, P.; Van Schepdael, A.; Law, S.-J. Mass and sequence verification of modified oligonucleotides using electrospray tandem mass spectrometry. *J. Mass Spectrom.* **1995,** *30,* 993–1006.
49. Iannitti, P.; Sheil, M. M.; Wickham, G. High sensitivity and fragmentation specificity in the analysis of drug-DNA adducts by electrospray tandem mass spectrometry. *J. Am. Chem. Soc.* **1997,** *119,* 1490–1491.
50. McCloskey, J. A.; Graham, D. E.; Zhou, S.; Crain, P. F.; Ibba, M.; Konisky, J.; Soll, D.; Olsen, G. J. Post-transcriptional modification in archaeal tRNAs: Identities and phylogenetic relations of nucleotides from mesophilic and hyperthermophilic Methanococcales. *Nucleic Acids Res.* **2001,** *29,* 4699–4706.
51. Kellersberger, K. A.; Yu, E.; Kruppa, G. H.; Young, M. M.; Fabris, D. Top-down characterization of nucleic acids modified by structural probes using high-resolution tandem mass spectrometry and automated data interpretation. *Anal. Chem.* **2004,** *76,* 2438–2445.
52. Gale, D. C.; Smith, R. D. Characterization of noncovalent complexes formed between minor groove binding molecules and duplex DNA by electrospray ionization-mass spectrometry. *J. Am. Soc. Mass Spectrom.* **1995,** *6,* 1154–1164.
53. Gabelica, V.; Rosu, F.; Houssier, C.; De Pauw, E. Gas phase thermal denaturation of an oligonucleotide duplex and its complexes with minor groove binders. *Rapid Commun. Mass Spectrom.* **2000,** *14,* 464–467.
54. Wan, K. X.; Gross, M. L.; Shibue, T. Gas-phase stability of double-stranded oligodeoxynucleotides and their noncovalent complexes with DNA-binding drugs as revealed by collisional activation in an ion trap. *J. Am. Soc. Mass Spectrom.* **2000,** *11,* 450–457.
55. David, W. M.; Brodbelt, J. S.; Kerwin, S. M.; Thomas, P. W. Investigation of quadruplex oligonucleotide-drug interaction by electrospray ionization mass spectrometry. *Anal. Chem.* **2002,** *74,* 2029–2033.
56. Mazzitelli, C. L.; Brodbelt, J. S.; Kern, J. T.; Rodriguez, M.; Kerwin, S. M. Evaluation of binding of perylene diimide and benzannulated perylene diimide ligands to DNA by electrospray mass spectrometry. *J. Am. Soc. Mass Spectrom.* **2006,** *17,* 593–604.
57. Griffey, R. H.; Greig, M. J.; Haoyun, A.; Sasmor, H.; Manalili, S. Targeted site-specific gas-phase cleavage of oligoribonucleotides. Application in mass spectrometry-based identification of ligand binding sites. *J. Am. Chem. Soc.* **1999,** *121,* 474–475.
58. Ni, J.; McCloskey, J. A.; Davis, D. R. *Proceedings of the 44th ASMS Conference on Mass Spectrometry and Allied Topics*; Portland, OR, 1996; p 325.
59. Gauthier, J. W.; Trautman, T. R.; Jacobson, D. B.Sustained off-resonance irradiation for collision-activated dissociation involving Fourier transform mass spectrometry. Collision-activated dissociation technique that emulates infrared multiphoton dissociation.Anal. Chim. Acta.2462111991225
60. de Koning, L. J.; Nibbering, N. M. M.; van Orden, S. L.; Laukien, F. H. Mass selection of ions in a Fourier transform ion cyclotron resonance trap using correlated harmonic excitation fields (CHEF). *Int. J. Mass Spectrom. Ion Processes* **1997,** *165/166,* 209–219.

61. Senko, M. W.; Speir, J. P.; McLafferty, F. W. Collisional activation of large multiply charged ions using Fourier transform mass spectrometry. *Anal. Chem.* **1994,** *66,* 2801–2808.
62. Morris, G. M.; Goodsell, D. S.; Halliday, R. S.; Huey, R.; Hart, W.; Belew, R. K.; Olson, A. J. Automated docking using a Lamarckian genetic algorithm and empirical binding free energy function. *J. Comp. Chem.* **1998,** *19,* 1639–1662.
63. Hagan, N.; Fabris, D. A direct mass spectrometric determination of the stoichiometry and binding affinity of the complexes between HIV-1 nucleocapsid protein and RNA stem-loops hairpins of the HIV-1 Ψ-recognition element. *Biochemistry* **2003,** *42,* 10736–10745.
64. Amarasinghe, G. K.; De Guzman, R. N.; Turner, R. B.; Summers, M. F. NMR structure of stem-loop SL2 of the HIV-1 psi RNA packaging signal reveals a novel A-U-A base-triple platform. *J. Mol. Biol.* **2000,** *299,* 145–156.
65. Pappalardo, L.; Kerwood, D. J.; Pelczer, I.; Borer, P. N. Three-dimensional folding of an RNA hairpin required for packaging HIV-1. *J. Mol. Biol.* **1998,** *282,* 801–818.
66. Kerwood, D. J.; Cavaluzzi, M. J.; Borer, P. N. Structure of SL-4 from the HIV-1 packaging signal. *Biochemistry* **2001,** *40,* 14518–14529.
67. Amarasinghe, G. K.; De Guzman, R. N.; Turner, R. B.; Chancellor, K. J.; Wu, Z. R.; Summers, M. F. NMR structure of the HIV-1 nucleocapsid protein bound to stem-loop SL2 of the Ψ-RNA packaging signal. Implications for genome recognition. *J. Mol. Biol.* **2000,** *301,* 491–511.
68. De Guzman, R. N.; Wu, Z. R.; Stalling, C. C.; Pappalardo, L.; Borer, P. N.; Summers, M. F. Structure of the HIV-1 nucleocapsid protein bound to the SL-3 Ψ-RNA recognition element. *Science* **1998,** *279,* 384–388.
69. Kirpekar, F.; Krogh, T. N. RNA fragmentation studied in a matrix-assisted laser desorption/ionization tandem quadrupole/orthogonal time-of-flight mass spectrometer. *Rapid Commun. Mass Spectrom.* **2001,** *15,* 8–14.
70. Tromp, J. M.; Schurch, S. Gas-phase dissociation of oligoribonucleotides and their analogs studied by electrospray ionization tandem mass spectrometry. *J. Am. Soc. Mass Spectrom.* **2005,** *16,* 1262–1268.
71. Fourmy, D.; Recht, M. I.; Blanchard, S. C.; Puglisi, J. D. Structure of the A-site of *E. coli* 16S rRNA complexed with an aminoglycoside antibiotic. *Science* **1996,** *274,* 1367–1371.
72. Busscher, G. F.; Rutjes, F. P. J. T.; van Delft, F. L. 2-Deoxystreptamine: Central scaffold of aminoglycoside antibiotics. *Chem. Rev.* **2005,** *105,* 775–791.
73. White, S. A.; Draper, D. E. Single base bulges in small RNA hairpins enhance ethidium binding and promote allosteric transition. *Nucleic Acids Res.* **1987,** *15,* 4049–4064.
74. D'Amico, M. L.; Paiotta, V.; Secco, F.; Venturini, M. A kinetic study of the intercalation of ethidium bromide into poly(A)·poly(U). *J. Phys. Chem. B* **2002,** *106,* 12635–12641.
75. Albert, F. G.; Eckdahl, T. T.; Fitzgerald, D. J.; Anderson, J. N. Heterogeneity in the actions of drugs that bind in the DNA minor groove. *Biochemistry* **1999,** *38,* 10135–10146.
76. Gabelica, V.; De Pauw, E. Comparison between solution-phase stability and gas-phase kinetic stability of oligodeoxynucleotide duplexes. *J. Mass Spectrom.* **2001,** *36,* 397–402.
77. Gabelica, V.; De Pauw, E. Comparison of the collision-induced dissociation of duplex DNA at different collision regimes: Evidence for a multistep dissociation mechanism. *J. Am. Soc. Mass Spectrom.* **2002,** *13,* 91–98.
78. Greco, F.; Liguori, A.; Sindona, G.; Uccella, N. Gas-phase proton affinity of deoxyribonucleosides and related nucleobases by fast atom bombardment tandem mass spectrometry. *J. Am. Chem. Soc.* **1990,** *112,* 9092–9096.
79. Abramovitz, D. L.; Pyle, A. M. Remarkable morphological variability of a common RNA folding motif: the GNRA tetraloop-receptor interaction. *J. Mol. Biol.* **1997,** *266,* 493–506.
80. Varani, G.; McClain, W. H.; The G·U wobble base pair. A fundamental building block of RNA structure crucial to RNA function in diverse biological systems. *EMBO Rep.* **2000,** *1,* 18–23.
81. Honig, B.; Nicholls, A. Classical electrostatics in biology and chemistry. *Science* **1995,** *268,* 1144–1149.
82. DeLano, W. L. The PyMOL Molecular Graphics System; DeLano Scientific: San Carlos, CA, 2002.